An Electrically Activated Nanobody Biosensor for On-Demand Detection

Williamson, Hannah K.; Mendes, Paula M.

DOI:
10.1021/acssensors.5c04140

Document Version
Publisher's PDF, also known as Version of record

Citation for published version (Harvard):
Williamson, HK & Mendes, PM 2026, 'An Electrically Activated Nanobody Biosensor for On-Demand Detection', *Sensors*, vol. 11, no. 2, pp. 1655-1662. https://doi.org/10.1021/acssensors.5c04140

ACS SENSORS

pubs.acs.org/acssensors
Article

An Electrically Activated Nanobody Biosensor for On-Demand Detection

Hannah K. Williamson and Paula M. Mendes*

Cite This: *ACS Sens.* 2026, 11, 1655−1662
Read Online

ABSTRACT: The development of systems capable of dynamic, on-demand target detection marks a transformative advance for biomanufacturing, diagnostics, and environmental monitoring. Nanobodies can recognize targets ranging from bacteria and proteins to small molecules, yet conventional platforms remain static, with perpetually exposed binding sites that hinder control in dynamic settings. We introduce an adaptive, on-demand sensing nanobody platform that leverages electrically responsive oligopeptides to gate antigen-binding sites between OFF (shielded) and ON (exposed) states. Upon electrical activation, binding sites are revealed with >80% efficiency, enabling real-time, selective detection. The system achieves pg/mL sensitivity over a broad dynamic range (pg/mL−μg/mL), performs reliably in serum and cell culture media, and supports multiplexed detection via independently addressable electrodes. This electroresponsive architecture defines a new paradigm for programmable, high-performance molecular detection.

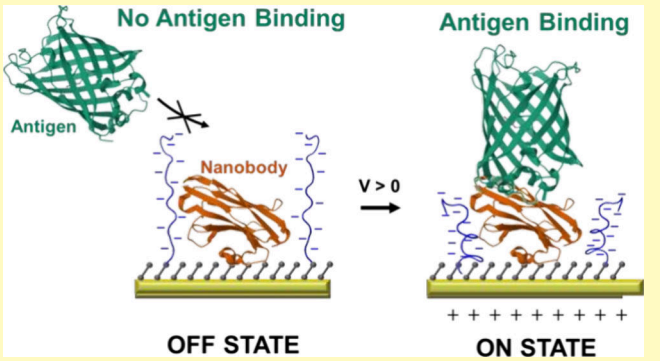

KEYWORDS: *on-demand sensing, nanobody, responsive peptides, electro-activation, self-assembled monolayers, dynamic systems*

Affinity-based electrochemical biosensors using biorecognition elements have enabled sensitive detection of a broad range of analytes, driving significant advances in healthcare diagnostics,[1] environmental monitoring,[2] and food safety.[3] Antibodies have long been used as biosensor recognition agents due to their high antigen-specificity,[4,5] however the fragility of their disulfide bonds[6] and larger size which limits surface coverage[7] have prompted investigation into superior options. Nanobodies, small and stable fragments derived from camelid heavy-chain antibodies, offer advantages over traditional antibodies, including improved thermal and chemical stability, smaller size (10−15 kDa), and higher affinity.[8,9] These beneficial properties enhance biosensor performance, making nanobodies particularly suitable for the detection of a wide array of targets, including bacteria,[10] proteins[11] and small molecules.[12] However, traditional biosensing systems rely on static configurations where nanobodies are continuously exposed to targets, thereby limiting spatio-temporal control of analyte binding.

Implementing on-demand target sensing - the precise control over sensing events in response to external stimuli - in nanobody-based systems holds considerable benefits across various fields. This includes enabling real-time, dynamic monitoring in areas such as biomanufacturing, where nanobodies could detect metabolites, proteins, antibodies and other critical markers, thereby enhancing process optimisation to ensure product quality.[13] In healthcare, continuous monitoring of disease markers using nanobody-based sensors would facilitate early diagnosis and personalised treatment strategies.[5,14−17] Additionally, in environmental diagnostics, on-demand target sensing offers the potential for the selective and rapid detection of pollutants - including heavy metals, organic toxins, and pathogens - improving the efficiency of environmental monitoring and enabling timely interventions.[18]

While the potential for on-demand sensing in nanobody-based systems is clear, achieving precise control over their dynamic interactions with targets remains a significant challenge. Existing on-demand sensing technologies have successfully used small biomolecules, such as sugars,[19,20] hormones,[21] and short peptides,[22−24] as biorecognition elements, with binding events regulated by external stimuli such as light or electrical potential changes. However, these approaches are inherently limited in detecting a broad spectrum of analytes compared to the vast target range of nanobodies. Extending such stimulus-responsive strategies to larger biomolecules like nanobodies introduces considerable complexity, stemming from their greater size, structural rigidity, and the challenge of modulating their high-affinity interactions without compromising stability, specificity, or functional integrity.

Received: November 4, 2025
Revised: December 16, 2025
Accepted: December 23, 2025
Published: February 6, 2026

https://doi.org/10.1021/acssensors.5c04140
ACS Sens. 2026, 11, 1655−1662

To address this challenge, we hypothesised that charged oligopeptides, which undergo reversible folding and unfolding on surfaces in response to electrical stimuli,[25,26] can be harnessed to modulate nanobody-target interactions. Here, we demonstrate the integration of nanobodies with electrically responsive oligopeptides on gold electrode surfaces, creating an electro-activated platform capable of precise spatiotemporal control over nanobody paratope exposure. Simultaneously, the modified electrodes support electrochemical sensing, providing a sensitive transduction method of binding events. This dual functionality represents a significant step forward in the development of adaptive, nanobody-based sensing systems.

BIOSENSOR FABRICATION

The underlying principle of our on-demand sensing strategy is illustrated in Figure 1, where a gold surface is transformed into an electrically activated OFF to ON nanobody-based sensor formed of a mixed monolayer of nanobody recognition elements and oligopeptide responsive units. By leveraging the net charge of the oligopeptides, control of their orientation in an applied electrical field through attraction or repulsion relative to the gold transducer surface confers OFF to ON antigen binding by occluding or revealing nanobody binding sites (Figure 1). To achieve this system, gold electrodes were first functionalised with a self-assembled monolayer (SAM) of 11-mercaptoundecanoic acid (11-MUA) to provide a reactive carboxylate group for subsequent conjugation. This is followed by carbodiimide chemistry to covalently co-immobilise both the nanobodies and the oligopeptides to the surface in a single step. The enhanced green fluorescent protein (eGFP) nanobody was selected as a model biorecognition element to demonstrate on-demand binding and electrochemical detection of a moderately-sized antigen (<30 kDa). Oligopeptides designed with negatively charged glutamic acid residues at physiological pH to facilitate conformational control under an applied electrical potential were chosen as the surface responsive units. These peptides featured a single terminal beta-alanine residue to enable site-directed coupling via carbodiimide chemistry, ensuring an upright orientation on the 11-MUA-functionalised surface. Conversely, the vast availability of primary amines on the nanobodies results in random orientations on the surface. The dimensions of these orientations were therefore considered when choosing the number of repeating glutamic acid residues required to maximise binding site occlusion by the oligopeptide responsive units. Initially, peptides formed of 7 residues (7EA) exhibited insufficient nanobody coverage to gain a complete OFF state (Figure S1). Consequently, an oligopeptide with an extended length (10EA) was used to ensure concealment of nanobody paratopes and achieve an OFF state at rest.

Electrochemical impedance spectroscopy (EIS) was used to confirm successful biofunctionalisation of Au electrodes through monitoring the electron transfer of the redox couple $[Fe(CN)_6]^{3-/4-}$ at the electrolyte solution-electrode surface interface. Interrogation of the validity of the data with Kramers-Kronig analysis revealed excellent correlation between experimental results and the Kramers-Kronig fit, with $\chi^2 < 0.00001$ for all surfaces. Nyquist plots were fit with the Randles equivalent circuit shown in Figure 2A, except bare Au where only Warburg diffusion was observed, showing excellent goodness of fit (solid lines). Consecutive functionalization steps resulted in significant increases in the resistance to charge transfer (R_{ct}) attributed to the physical

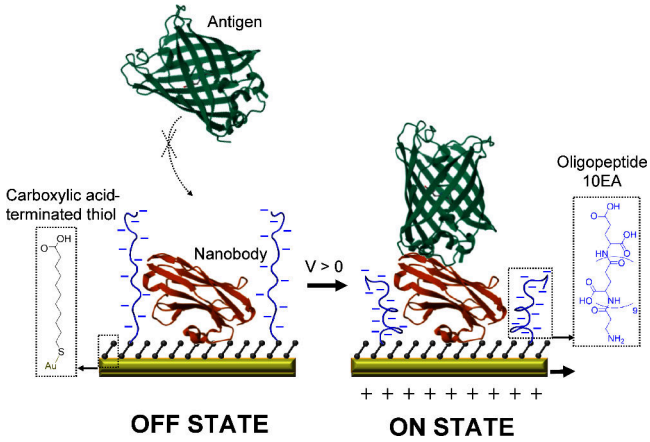

Figure 1. An electrically activated nanobody-based biosensor for on-demand electrochemical sensing. Nanobodies and negatively charged oligopeptides in a mixed solution are immobilised on a carboxylic acid-terminated thiol (11-MUA) SAM functionalised gold electrode. At open circuit potential (OCP), oligopeptides are extended beyond nanobody binding sites, preventing antigen (eGFP) binding and establishing an OFF state. Application of a positive potential attracts the oligopeptides to the electrode surface, revealing nanobody binding sites and allowing antigen binding in the ON state.

blocking and electrostatic repulsion of the redox couple which reduces faradaic currents. As a technique particularly sensitive to surface charge, EIS revealed a direct correlation between the peptide solution ratio and the resulting surface peptide density. This was evidenced by the positive relationship between the R_{ct} and the increasing concentration of 10EA on the surface (Figure 2A). For pure nanobody surfaces (1:0), R_{ct} was measured at 1204 ± 191 kΩ. Introducing 10EA resulted in a progressive increase in R_{ct}, reaching 1968 ± 270 kΩ at the 1:1 ratio, 2365 ± 621 kΩ at 1:2, 3908 ± 1962 kΩ at 1:5, and 6305 ± 866 kΩ for pure 10EA surfaces (0:1). This increase in R_{ct} can be attributed to the repulsion of the negatively charged $[Fe(CN)_6]^{3-/4-}$ redox probe by the net negative charge of 10EA at physiological pH, which hinders electron transfer at the electrochemical interface.

NANOBODY OFF TO ON ACTIVATION

A potential of +0.3 V was selected as the activation potential because it lies within the established electrochemical stability window of peptide- and thiol-based self-assembled monolayers. Prior studies[25−27] on structurally analogous peptide systems have shown that monolayer integrity is retained at +0.3 V, whereas higher positive potentials lead to perturbation of the SAM and the onset of thiol desorption. Lower activation potentials have also been reported to be insufficient, with +0.2 V yielding markedly reduced activation efficiencies (<5%) in related electro-responsive peptide interfaces.[28] Taken together, these findings identify +0.3 V as the optimal activation potential that preserves SAM stability while providing sufficient electrostatic driving force to induce the peptide collapse required for functional activation.

To explore the OFF to ON electro-activation capability of nanobody:oligopeptide surfaces, eGFP incubation was initially performed under open circuit potential (OCP) in buffer, followed by EIS measurement in redox solution. Stabilisation under +0.3 V in buffer was achieved, and a subsequent antigen incubation at

https://doi.org/10.1021/acssensors.5c04140
ACS Sens. 2026, 11, 1655−1662

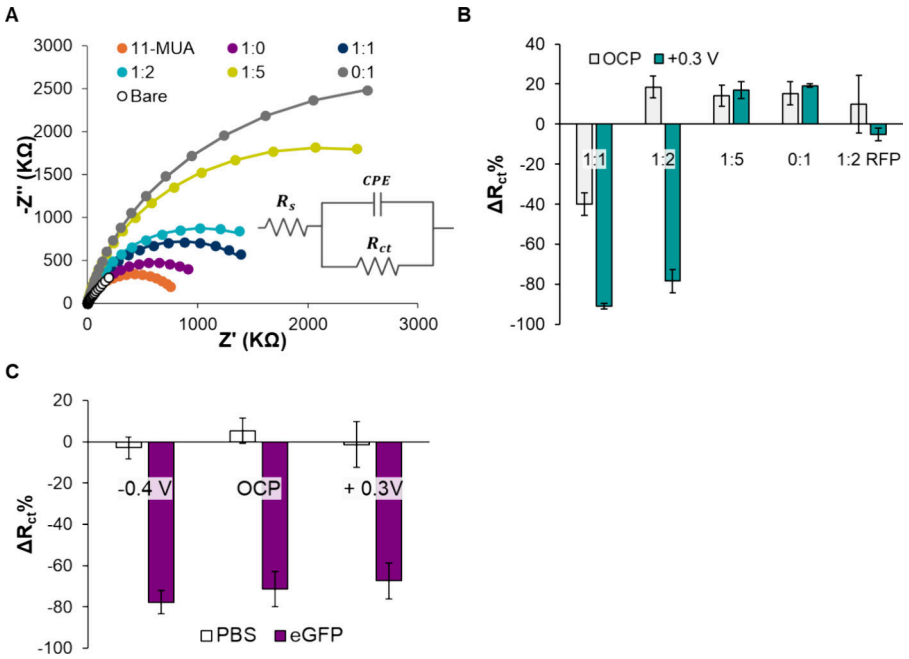

Figure 2. Nb:10EA OFF to ON electro-activated surfaces. (A) Nyquist plots of Bare Au, 11-MUA, Nb-only (1:0), Nb:10EA (1:1; 1:2; 1:5) and 10EA-only (0:1) functionalised electrodes fitted with the equivalent circuit model depicted. Nyquists are representative of the average ($n \geq 5$). (B) Response (ΔR_{ct}%) of 1:1, 1:2 and 1:5 Nb:10EA, and 10EA-only electro-activated biosensors after eGFP incubation at OCP and under +0.3 V. Error bars show standard deviation ($n = 3$). (C) Response of always-ON Nb-only biosensors after PBS or eGFP incubation at OCP and under −0.4 V or +0.3 V. Error bars show standard deviation ($n = 3$).

the same potential demonstrated the capacity of each surface to undergo OFF to ON activation.

The ΔR_{ct}% (Eq. S1) between PBS baseline and post-eGFP incubation was reported as the biosensor response. At the 1:1 Nb:10EA ratio, a biosensor response of −40 ± 6% at OCP indicated partial antigen binding prevention, indicating that a complete OFF state was not achieved (Figure 2B). The electro-activation efficiency (Eq. S2) at the 1:1 Nb:10EA ratio reached 85%, with a significant decrease in response to −91 ± 2% under +0.3 V. This performance surpasses the binding response observed for a pure nanobody surface at OCP, which exhibited an average response of −71 ± 8% following eGFP incubation. At this ratio, the introduction of the oligopeptides in the mixed surface therefore acted to improve the spatial arrangement of nanobodies for antigen binding in the ON state rather than fully concealing all available paratopes in the OFF state.

Given the partial concealment at the 1:1 ratio, higher concentrations of 10EA were subsequently investigated. At OCP, the 1:2 and 1:5 Nb:10EA biosensors demonstrate responses of 19 ± 6% and 14 ± 5%, respectively, suggesting the absence of eGFP binding (Figure 2B). The higher concentrations of 10EA therefore provided sufficient concealment of nanobody binding sites at OCP, where it is thought that increased surface densities maintained an upright oligopeptide conformation through electrostatic repulsion, with oligopeptides extending beyond nanobody binding sites to establish a complete OFF state. Upon application of +0.3 V, the 1:5 ratio exhibits a minimal response change (17 ± 4%, $p > 0.05$), showing a lack of OFF to ON activation. In contrast, the 1:2 ratio shows a marked decrease to −78 ± 6% ($p < 0.01$), demonstrating successful electro-activation with an efficiency of 80%.

These results indicate that the increased density of 10EA at the 1:5 ratio likely creates a steric barrier, preventing oligopeptide collapse and maintaining occlusion of the nanobody binding sites. In contrast, at the 1:2 Nb:10EA ratio, applying a positive electrochemical potential (+0.3 V) enabled transition from the OFF state where oligopeptide extension blocked nanobody binding sites, to a collapsed surface nanoarchitecture due to oligopeptide electrostatic attraction to the surface, exposing the binding sites and enabling antigen binding, as detected by EIS. It is expected that similar surface dynamics occur as seen with other surface architectures designed to enable a similar activation mechanism.[26,27,29]

As the biosensor exhibits an R_{ct} decrease after eGFP incubation, we sought to confirm the specificity of this response to nanobody-target binding. As orthogonal techniques to electrochemistry, fluorescence and surface plasmon resonance confirmed the occurrence of specific native binding of eGFP to always-ON nanobody pure surfaces (Figure S2). In support of specific binding occurring in the electrochemical system, the usual change in R_{ct} was not exhibited for oligopeptide pure surfaces when eGFP was incubated at OCP (15 ± 6%) or +0.3 V (19 ± 1 %) (Figure 2B). Furthermore, binding responses of the negative control RFP (Red Fluorescent Protein) (Figure 2B) on 1:2 Nb:10EA surfaces at open-circuit potential (OCP; 10 ± 15%) were not significantly different from those of eGFP at OCP (19 ± 6%; $p > 0.05$), suggesting minimal background interactions with the surface. However, at +0.3 V, a significant difference was observed between the RFP response (−5 ± 3 %) and the eGFP response (−78 ± 6%; $p < 0.01$), validating the electrochemical response as antigen-specific. Additional confirmation that changes in R_{ct} result from antigen binding rather than surface degradation was obtained by subjecting the electrodes to +0.3 V for 60 min and assessing % changes in peak current (I_p) and R_{ct} over time (Figure S3). Negligible changes in I_p were observed, with individual electrodes exhibiting variations of < ±6% over the measured time, while average R_{ct} values remained below 10% after 60 min under +0.3 V, confirming surface stability and verifying that bioreceptor dissociation due to potential application does not underly the

https://doi.org/10.1021/acssensors.5c04140
ACS Sens. 2026, 11, 1655−1662

decrease in R_{ct}. The biosensor response to eGFP at OCP, +0.3 V and −0.4 V was also evaluated for always-ON Nb sensors devoid of oligopeptides. Blank phosphate buffered saline (PBS) incubations resulted in negligible responses (< ±10%) while responses of −78 ± 3%, −71 ± 8% and −66 ± 10% at −0.4 V, OCP and +0.3 V for eGFP, respectively showed no statistically significant difference ($p > 0.1$) (Figure 2C). Modulation of nanobody-antigen binding is therefore directly imparted by the presence and action of the oligopeptides rather than potential-driven antigen attraction or repulsion by the electric field. In physiological ionic strength, the electric field decays exponentially outside of the Debye length (<1 nm),[30] and its influence in the bulk solution is negligible. Although only the interfacial region near the tethered end of the peptide experiences the applied potential, this local perturbation at the anchoring point causes the entire peptide to reorganise, as the chain conformation adjusts collectively through electrostatic and steric interactions. These findings confirmed that the biosensor response results from electrically induced activation of the oligopeptide layer, which exposed the nanobody binding sites, rather than from any long-range field effects on the antigen.

SENSOR CHARACTERISTICS

With a Nb:10EA ratio of 1:2 discovered as the optimal surface architecture for OFF to ON activation, further surface characterization was performed. The 1:2 Nb:10EA biosensor exhibits hydrophilic characteristics, with an advancing contact angle of 66 ± 5° and a receding contact angle of 16 ± 3°, both of which are intermediate values between those measured for pure 10EA and pure nanobody functionalised surfaces (Table S2). The sensor's surface thickness of 3.0 ± 0.4 nm also falls within the range observed for the individual components (Table S2). X-ray photoelectron spectroscopy (XPS) provides additional compositional evidence, confirming the formation of a Nb:10EA mixed monolayer surface. High-resolution XPS spectra for Au 4f, C 1s, O 1s, N 1s, and S 2p were obtained for 11-MUA, Nb-only, 1:2 Nb:10EA, and pure 10EA surfaces (Figure S4). High-resolution XPS analysis reveals significant increases in C:Au, N:Au, and O:Au ratios for nanobody-only ($p < 0.01$), Nb:10EA ($p < 0.01$), and 10EA-only ($p < 0.05$) surfaces compared to 11-MUA (Table S3). N:Au ratios for nanobody-only and Nb:10EA surfaces are significantly increased ($p < 0.01$) compared to those of 10EA-only surfaces, reflecting the higher globular structural complexity of nanobody proteins compared to short-chain oligopeptides. This complexity is further demonstrated by the increased ratios of C:Au and O:Au for nanobody-only and Nb:10EA surfaces compared to those of 10EA-only surfaces. Moreover, higher relative percentages of C=O and C-O components associated with carboxylic acid groups from amino acids such as glutamic acid, aspartic acid, and serine are observed on nanobody-containing surfaces compared to 10EA-only surfaces. Further analysis of the S 2p region identifies free thiol contributions from methionine and cysteine residues in the nanobody,[31] while a significantly reduced S:Au ratio ($p < 0.01$) for Nb:10EA surfaces compared to nanobody-only surfaces indicates fewer immobilised nanobodies due to 10EA occupying surface space. By considering the total amount of nitrogen and the expected contributions of nitrogen and sulfur atoms by each component in Nb:10EA surfaces (Eq. S3), the Nb:10EA ratio is calculated as 7:1, differing from the solution ratio of 1:2. This discrepancy arises from differences in adsorption efficiency of the nanobodies and oligopeptides during co-immobilisation.[25,28] Negatively charged 10EA peptides pack less efficiently on the surface due to electrostatic repulsion and conformational constraints, whereas nanobodies, with multiple available lysine residues for coupling, immobilise more readily. As a result, the surface composition is enriched in nanobodies compared to oligopeptides. This XPS derived ratio supports the need for a relatively low peptide ratio to effectively conceal the nanobodies on the surface when a peptide of sufficient length is used, further suggesting that peptide length-induced steric hindrance of paratopes is the primary mechanism underlying the OFF state.

EVALUATION OF BIOSENSOR PERFORMANCE

We next evaluated the biosensor's dynamic activation and antigen detection capabilities in biochemically relevant solutions, including PBS and RPMI medium. The 1:2 Nb:10EA biosensors were stabilised in the appropriate matrix before eGFP incubation at OCP. After washing and EIS measurement, the sensors were stabilised at +0.3 V, followed by eGFP incubation under potential. Post-wash, EIS was performed. As shown in Figure 3A, direct electro-activation from the OFF state at OCP to the ON state at +0.3 V was preserved across all concentrations in PBS. At OCP, higher non-specific responses were observed at high ng mL^{-1} to low μg mL^{-1} concentrations (11−16%), likely due to antigen saturation of the surface leading to non-specific interactions with oligopeptides. However, this did not affect nanobody functionality or activation performance. Interestingly, non-specific binding was not observed in RPMI, possibly due to the medium's complexity and lower pH (pH 6.8), which might hinder antigen-oligopeptide interactions (Figure 3B).

Biosensor performance across both matrices and always-ON Nb biosensors in PBS (Figure S5) revealed that electro-activated biosensors demonstrated significantly enhanced sensitivity (Table 1). This improvement is evidenced by lower limits of detection (LoD) and quantification (LoQ), as calculated from the steeper response slope. Moreover, the dynamic range of the electro-activated biosensors was extended by 100-fold. This extended range originates from the mixed Nb:10EA nanoarchitecture, where the oligopeptides introduce additional spacing between neighbouring nanobody molecules and thereby reduce steric crowding at the surface. Enhanced accessibility to the binding sites enables antigen recognition to be sustained over a wider concentration span before steric saturation occurs, consistent with reports of similar behaviour in other surface-based biosensors.[32,33] The biosensor nanoarchitecture therefore not only enabled on-demand sensing but improved overall sensing capability.

One area where on-demand detection of protein analytes is becoming a necessity is in the bioprocessing of cell and gene therapies.[13] To highlight the possible capability of our biosensor for this use, on-demand sensing of eGFP antigen was tested in cell supernatant samples from pluripotent stem cell bioreactor cultures with high and low cell densities. Samples were spiked with either 14 ng mL^{-1} or 14 μg mL^{-1}, corresponding to the mid-to-high range of the biosensor. For low cell density samples, the OFF state was successfully established with responses of −7 ± 3% and 15 ± 3% for 14 ng mL^{-1} and 14 μg mL^{-1}, respectively (Figure 3C). Following electro-activation, responses of −32 ± 9% and −84 ± 5% exhibited concentration dependent detection. Similar results were observed in high cell density samples, where responses at OCP were −1 ± 4% and 12 ± 13%, confirming the absence of eGFP binding in the OFF state. Activation to the ON state enabled antigen binding, with responses of −28 ± 5%

https://doi.org/10.1021/acssensors.5c04140
ACS Sens. 2026, 11, 1655−1662

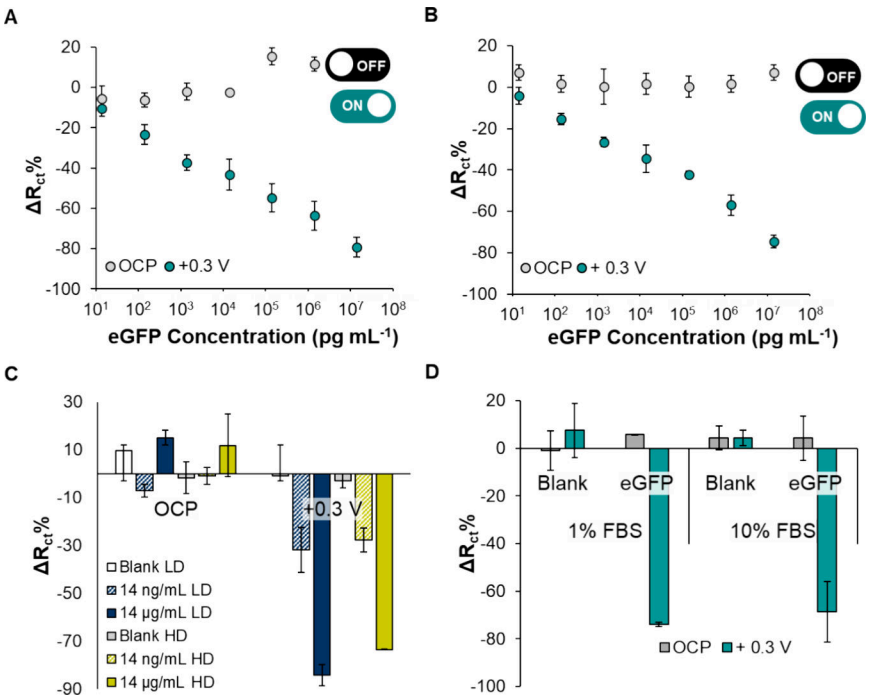

Figure 3. Biosensor performance in complex media. Concentration response curves for the 1:2 Nb:10EA electro-activated biosensor with eGFP antigen in (A) PBS and (B) RPMI media. Antigen incubation was performed first at OCP (grey) and then at +0.3 V (green). Error bars represent the standard deviation ($n = 3$). (C) Biosensor response to PBS and eGFP antigen spiked samples derived from low density (LD) and high density (HD) pluripotent stem cell cultures at OCP and +0.3 V. Error bars show standard deviation ($n = 3$). (D) Biosensor electro-activated in PBS or 14 µg mL^{-1} eGFP spiked 1% and 10% FBS. Error bars show standard deviation ($n = 3$).

Table 1. Biosensor sensitivity comparison in complex media[a]

	NbGFP Biosensor (PBS)	Nb:10EA Biosensor (PBS)	Nb:10EA Biosensor (RPMI)
LoD	7.6 pg mL^{-1}	4.5 pg mL^{-1}	5.0 pg mL^{-1}
LoQ	23.1 pg mL^{-1}	13.7 pg mL^{-1}	15.2 pg mL^{-1}
Dynamic Range	14 pg mL^{-1}–140 ng mL^{-1}	14 pg mL^{-1}–14 µg mL^{-1}	14 pg mL^{-1}–14 µg mL^{-1}
Slope	−3.632	−4.733	−4.81
Linearity (R^2)	0.949	0.991	0.982

[a]Comparison of the limit of detection (LoD), limit of quantification (LoQ), dynamic range, slope and linearity extracted from antigen calibration curves for NbGFP-only and 1:2 Nb:10EA in PBS and RMPI media.

and −73.4 ± 0.2% for 14 ng mL^{-1} and 14 µg mL^{-1}, respectively. Cell samples spiked with blank PBS did not result in significant changes in R_{ct} upon electro-activation, supporting the specificity of the electrochemical responses to eGFP binding rather than matrix effects or signal decay. The platform was further tested in complex matrices, including 1% and 10% fetal bovine serum (FBS) in PBS (Figure 3D). With 14 µg mL^{-1} eGFP spiked into 1% FBS, the biosensor maintained effective performance, with response changes from 5.7 ± 0.1% at OCP to −73.9 ± 0.9%, resulting in a high signal-to-noise ratio (74.6). In 10% FBS, while electro-activation was still observed, the response changes from 4 ± 9% at OCP to −69 ± 13% at +0.3 V showed a reduced signal-to-noise ratio (5.1), indicating greater interference from the complex matrix. To investigate the impact of FBS on biosensor performance, electro-activation was also tested with 14 µg mL^{-1} RFP spiked into 10% FBS as a non-specific control (Figure S6). The RFP and eGFP responses at OCP were not significantly different ($p > 0.1$), confirming that the oligopeptides effectively shielded the Nb binding sites from serum proteins, preserving the OFF state in FBS. Upon electro-activation, the RFP response remained significantly lower ($p < 0.05$) compared to eGFP in the ON state. There were no significant differences between the RFP responses at OCP and +0.3 V ($p > 0.05$), nor between the ON responses in PBS and 10% FBS ($p > 0.1$). However, similar to eGFP, the RFP ON response exhibited significant noise (105% %CV), indicating matrix interference. Overall, these results demonstrate that while FBS-induced matrix interference introduced some variation, it did not impact the overall antigen detection performance. Investigation of the biosensor performance in other complex matrices such as whole blood and plasma is therefore warranted to understand whether the responsive surface could offer on-demand detection of disease markers.

■ ON-DEMAND SENSING IN A MULTIARRAY

To investigate the feasibility of electro-activated biosensors for multiplexed, on-demand sensing, we utilised screen-printed multi-electrode arrays (SPEs), each comprising four gold

https://doi.org/10.1021/acssensors.5c04140
ACS Sens. 2026, 11, 1655−1662

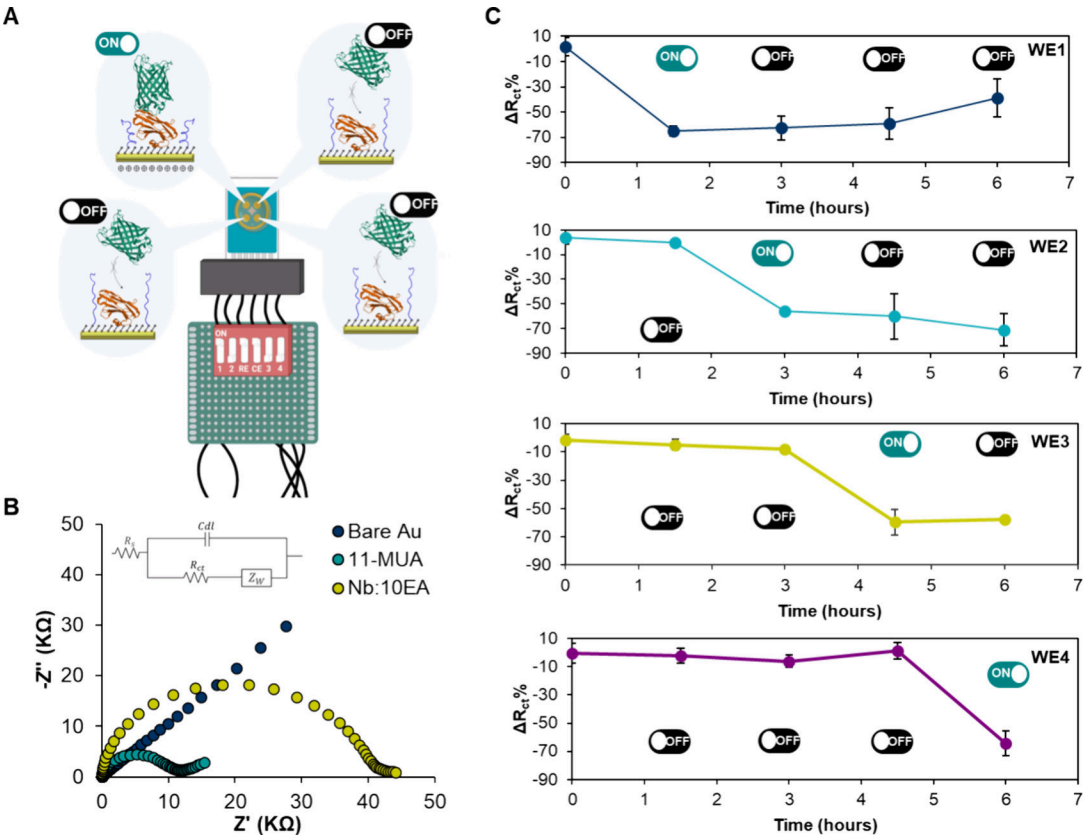

Figure 4. On-demand biosensing with Nb:10EA electro-activated arrays. (A) Individual working electrodes (WEs) on an array functionalised with 1:2 Nb:10EA electro-activated surfaces to build a biosensor platform capable of multiplexed on-demand detection. (B) Nyquist plots of bare Au, 11-MUA and Nb:10EA 1:2 functionalised arrays and the Randles equivalent circuit model used to fit the data. Nyquists are representative of at least 4 individual electrodes. (C) The ΔR_{ct}% of each WE of the biosensor platform in response to eGFP incubation performed every 1.5 hours. Each WE was individually electro-activated by applying +0.3 V which is indicated by the green ON state cartoon. The black OFF state cartoon indicates an antigen incubation performed at OCP. Error bars show standard deviation ($n \geq 3$).

working electrodes (WEs) (Figure 4A). A custom-engineered platform, incorporating a single-channel potentiostat and a switch box connected via a printed circuit board (Figure S7), enabled precise and independent control of individual electrodes. Electrochemical characterisation at each functionalisation step confirmed the successful fabrication of the biosensor on Au SPE arrays (Figure 4A; Figure S7A). Furthermore, a linear relationship ($R^2 = 0.9999$) between I_{pa} and $\sqrt{}$scan rate for bare Au SPEs was indicative of a diffusion controlled process aligning with the Randles-Sevcik equation, confirming the successful function of the electrical hardware (Figure S7C).

Over a 6 hour period, the four WEs were sequentially activated for selective eGFP detection. At 1.5 hour intervals, a single electrode was activated by applying +0.3 V versus an external Pt wire counter electrode (CE), while the remaining electrodes were held at open-circuit potential (OCP) to preserve their inactive state. Following stabilisation in PBS, all electrodes underwent a 15 minute incubation with 14 μg mL^{-1} eGFP. Changes in R_{ct} were recorded at each time point for each electrode, reflecting their ON/OFF states. As shown in Figure 4C, the OFF state was consistently maintained for all inactive electrodes, while activated electrodes exhibited significant shifts in R_{ct}, demonstrating successful and selective eGFP binding. Importantly, the oligopeptide shielding of nanobody binding sites effectively prevented non-specific interactions throughout the experiment, as evidenced by the consistent performance of WE 4, the last electrode to be activated. The robust and reproducible electro-activated process enabled precise, sequential, on-demand sensing across the entire electrode array.

We developed an electrochemical biosensor platform that leverages electrically responsive oligopeptides to dynamically control nanobody binding sites, transitioning them from an inactive OFF to an active ON state. With an electro-activation efficiency of 80%, this system offers unprecedented pr ecision in biomolecular detection, minimising non-specific interactions while enabling real-time, targeted sensing. The platform demonstrated high sensitivity (pg mL^{-1}) across a wide dynamic range (pg mL^{-1} to μg mL^{-1}) and maintained robust performance in complex biological matrices, including serum. Its ability to independently activate sensing surfaces at specific time intervals enables precise, on-demand sensing, offering a versatile solution for applications in bioprocessing, healthcare diagnostics, and environmental monitoring.

■ ASSOCIATED CONTENT

Data Availability

All the data needed to understand and assess the conclusions are available in the main text and supplementary materials.

Supporting Information

The Supporting Information is available free of charge at https://pubs.acs.org/doi/10.1021/acssensors.5c04140.

https://doi.org/10.1021/acssensors.5c04140
ACS Sens. 2026, 11, 1655−1662

Materials and methods, supplementary text, Figures S1 to S7, and Tables S1 to S3 (DOCX)

AUTHOR INFORMATION

Corresponding Author

Paula M. Mendes − *School of Chemical Engineering, University of Birmingham, Birmingham B15 2TT, UK;* Email: p.m.mendes@bham.ac.uk

Author

Hannah K. Williamson − *School of Chemical Engineering, University of Birmingham, Birmingham B15 2TT, UK*

Complete contact information is available at: https://pubs.acs.org/doi/10.1021/acssensors.5c04140

Author Contributions

P.M. conceived the project. H.W. conducted the experimental work and analysed the data, under the supervision of P.M. H.W. and P.M. wrote the manuscript.

Funding

Thanks are given to Engineering and Physical Sciences Research Council EP/V041843/1 (P.M.) and Engineering and Physical Sciences Research Council EP/S02347X/1 (H.W., P.M.).

Notes

P.M. holds a patent related to the technology discussed in this manuscript (WO2018185503). The authors declare no other competing interests.

ACKNOWLEDGMENTS

We gratefully acknowledge the UK Cell and Gene Therapy Catapult for culturing and providing the pluripotent stem cell supernatants used in this study.

REFERENCES

(1) Campuzano, S.; Pedrero, M.; Torrente-Rodríguez, R. M.; Pingarrón, J. M. Affinity-based wearable electrochemical biosensors: Natural versus biomimetic receptors. *Anal. Sens.* **2023**, *3*. No. e202200087.

(2) Gavrilas, S.; Ursachi, C. S.; Perta-Crisan, S.; Munteanu, F. D. Recent trends in biosensors for environmental quality monitoring. *Sensors* **2022**, *22*, 1513.

(3) Curulli, A. Electrochemical biosensors in food safety: Challenges and perspectives. *Molecules* **2021**, *26*, 2940.

(4) van Oss, C. J.; Good, R. J.; Chaudhury, M. K. Nature of the antigen-antibody interaction: Primary and secondary bonds: Optimal conditions for association and dissociation. *J. Chromatogr. B: Biomed. Sci. Appl.* **1986**, *376*, 111–119.

(5) Zhang, Y.; Fan, F.; Chai, Y.; Chen, X. Biosensing materials for monoclonal antibody detection: An overview. *Responsive Mater.* **2024**, *2*, No. e20240006.

(6) Tiede, C.; Tang, A. A. S.; Deacon, S. E.; Mandal, U.; Nettleship, J. E.; Owen, R. L.; George, S. E.; Harrison, D. J.; Owens, R. J.; Tomlinson, D. C.; McPherson, M. J. Adhiron: a stable and versatile peptide display scaffold for molecular recognition applications. *Protein Eng., Des. Sel.* **2014**, *27*, 145–155.

(7) Gebauer, M.; Skerra, A. Engineered protein scaffolds as next-generation antibody therapeutics. *Curr. Opin. Chem. Biol.* **2009**, *13*, 245–255.

(8) Tiede, C.; Bedford, R.; Heseltine, S. J.; Smith, G.; Wijetunga, I.; Ross, R.; Al Qallaf, D.; Roberts, A. P. E.; Balls, A.; Curd, A.; Hughes, R. E.; Martin, H.; Needham, S. R.; Zanetti-Domingues, L. C.; Sadigh, Y.; Peacock, T. P.; Tang, A. A.; Gibson, N.; Kyle, H.; Platt, G. W.; Ingram, N.; Taylor, T.; Coletta, L. P.; Manfield, I.; Knowles, M.; Bell, S.; Esteves, F.; Maqbool, A.; Prasad, R. K.; Drinkhill, M.; Bon, R. S.; Patel, V.; Goodchild, S. A.; Martin-Fernandez, M.; Owens, R. J.; Nettleship, J. E.; Webb, M. E.; Harrison, M.; Lippiat, J. D.; Ponnambalam, S.; Peckham, M.; Smith, A.; Ferrigno, P. K.; Johnson, M.; McPherson, M. J.; Tomlinson, D. C. Affimers proteins are versatile and renewable affinity reagents. *eLife* **2017**, *6*, No. e24903.

(9) Muyldermans, S. Nanobodies: Natural Single-Domain Antibodies. In *Annual Review of Biochemistry*; Kornberg, R. D. Ed.; Annual Review of Biochemistry, 2013; Vol. *82*,; pp 775-797, 10.1146/annurev-biochem-063011-092449.

(10) Dhehibi, A.; Allaoui, A.; Raouafi, A.; Terrak, M.; Bouhaouala-Zahar, B.; Hammadi, M.; Raouafi, N.; Salhi, I. Nanobody-based sandwich immunoassay for pathogenic *Escherichia coli* F17 strain detection. *Biosensors* **2023**, *13*, 299.

(11) Guo, K. Y.; Wustoni, S.; Koklu, A.; Díaz-Galicia, E.; Moser, M.; Hama, A.; Alqahtani, A. A.; Ahmad, A. N.; Alhamlan, F. S.; Shuaib, M.; Pain, A.; McCulloch, I.; Arold, S. T.; Grünberg, R.; Inal, S. Rapid single-molecule detection of COVID-19 and MERS antigens via nanobody-functionalized organic electrochemical transistors. *Nat. Biomed. Eng.* **2021**, *5*, 666–677.

(12) El-Moghazy, A. Y.; Huo, J. Q.; Amaly, N.; Vasylieva, N.; Hammock, B. D.; Sun, G. An innovative nanobody-based electrochemical immunosensor using decorated nylon nanofibers for point-of-care monitoring of human exposure to pyrethroid insecticides. *ACS Appl. Mater. Interfaces* **2020**, *12*, 6159–6168.

(13) Williamson, H. K.; Mendes, P. M. An integrated perspective on measuring cytokines to inform CAR-T bioprocessing. *Biotechnol. Adv.* **2024**, *75*, No. 108405.

(14) Barbone, A. S.; Meftah, M.; Markiewicz, K.; Dellimore, K. Beyond wearables and implantables: a scoping review of insertable medical devices. *Biomed. Phys. Eng. Express* **2019**, *5*, No. 062002.

(15) Boscari, F.; Vettoretti, M.; Cavallin, F.; Amato, A. M. L.; Uliana, A.; Vallone, V.; Avogaro, A.; Facchinetti, A.; Bruttomesso, D. Implantable and transcutaneous continuous glucose monitoring system: a randomized cross over trial comparing accuracy, efficacy and acceptance. *J. Endocrinol. Invest.* **2022**, *45*, 115–124.

(16) Tang, Y.; Xiang, D.; Li, Q. In Situ Secondary Self-Assembly of Near-Infrared II J-Aggregates: A Novel Phototheranostic Strategy for Inducing Tumor Pyroptosis. *Adv. Mater.* **2025**, *37*, No. 2501184.

(17) Tang, Y.; Wang, X.; Chen, S.; Li, Q. Photoactivated theranostic nanomaterials based on aggregation-induced emission luminogens for cancer photoimmunotherapy. *Responsive Mater.* **2024**, *2*, No. e20240003.

(18) Gavrilaș, S.; Ursachi, C. Ș.; Perța-Crișan, S.; Munteanu, F.-D. Recent trends in biosensors for environmental quality monitoring. *Sensors* **2022**, *22*, 1513.

(19) Zhang, J.; Ma, W.; He, X. P.; Tian, H. Taking orders from light: Photo-switchable working/inactive smart surfaces for protein and cell adhesion. *ACS Appl. Mater. Interfaces* **2017**, *9*, 8498–8507.

(20) Weber, T.; Chandrasekaran, V.; Stamer, I.; Thygesen, M. B.; Terfort, A.; Lindhorst, T. K. Switching of bacterial adhesion to a glycosylated surface by reversible reorientation of the carbohydrate ligand. *Angew. Chem. Int. Ed.* **2014**, *53*, 14583–14586.

(21) Gomes, B. S.; Cantini, E.; Tommasone, S.; Gibson, J. S.; Wang, X. Y.; Zhu, Q.; Ma, J.; McGettrick, J. D.; Watson, T. M.; Preece, J. A.; Kirkman-Brown, J. C.; Publicover, S. J.; Mendes, P. M. On-demand electrical switching of antibody-antigen binding on surfaces. *ACS Appl. Bio Mater.* **2018**, *1*, 738–747.

(22) Lashkor, M.; Rawson, F. J.; Stephenson-Brown, A.; Preece, J. A.; Mendes, P. M. Electrically-driven modulation of surface-grafted RGD peptides for manipulation of cell adhesion. *Chem. Commun.* **2014**, *50*, 15589–15592.

(23) Kadem, L. F.; Holz, M.; Suana, K. G.; Li, Q.; Lamprecht, C.; Herges, R.; Selhuber-Unkel, C. Rapid reversible photoswitching of integrin-mediated adhesion at the single-cell level. *Adv. Mater.* **2016**, *28*, 1799–1802.

(24) Ng, C. C. A.; Magenau, A.; Ngalim, S. H.; Ciampi, S.; Chockalingham, M.; Harper, J. B.; Gaus, K.; Gooding, J. J. Using an

electrical potential to reversibly switch surfaces between two states for dynamically controlling cell adhesion. *Angew. Chem. Int. Ed.* **2012**, *51*, 7706–7710.
(25) Yeung, C. L.; Iqbal, P.; Allan, M.; Lashkor, M.; Preece, J. A.; Mendes, P. M. Tuning specific biomolecular interactions using electro-switchable oligopeptide surfaces. *Adv. Funct. Mater.* **2010**, *20*, 2657–2663.
(26) Yeung, C. L.; Wang, X. Y.; Lashkor, M.; Cantini, E.; Rawson, F. J.; Iqbal, P.; Preece, J. A.; Ma, J.; Mendes, P. M. Modulation of biointeractions by electrically switchable oligopeptide surfaces: structural requirements and mechanism. *Adv. Mater. Interfaces* **2014**, *1*, No. 1300085.
(27) Gibson, J. S.; Mendes, P. M. Elucidating the Influence of Electrical Potentials on the Formation of Charged Oligopeptide Self-Assembled Monolayers on Gold. *ChemPhysChem* **2021**, *22*, 684–692.
(28) Santos Gomes, B.; Cantini, E.; Tommasone, S.; Gibson, J. S.; Wang, X.; Zhu, Q.; Ma, J.; McGettrick, J. D.; Watson, T. M.; Preece, J. A.; Kirkman-Brown, J. C.; Publicover, S. J.; Mendes, P. M. On-Demand Electrical Switching of Antibody–Antigen Binding on Surfaces. *ACS Appl. Bio Mater.* **2018**, *1*, 738–747.
(29) Pranzetti, A.; Davis, M.; Yeung, C. L.; Preece, J. A.; Koelsch, P.; Mendes, P. M. Direct Observation of Reversible Biomolecule Switching Controlled By Electrical Stimulus. *Adv. Mater. Interf.* **2014**, *1*, No. 1400026.
(30) Kesler, V.; Murmann, B.; Soh, H. T. Going beyond the Debye Length: Overcoming Charge Screening Limitations in Next-Generation Bioelectronic Sensors. *ACS Nano* **2020**, *14*, 16194–16201.
(31) *GFP-nanobody in PDB entry 3ogo PDBe EMBL-EBI*, https://www.ebi.ac.uk/pdbe/entry/pdb/3ogo/protein/2.
(32) González-Fernández, E.; Staderini, M.; Avlonitis, N.; Murray, A. F.; Mount, A. R.; Bradley, M. Effect of spacer length on the performance of peptide-based electrochemical biosensors for protease detection. *Sens. Actuators, B* **2018**, *255*, 3040–3046.
(33) Zorea, J.; Shukla, R. P.; Elkabets, M.; Ben-Yoav, H. Probing antibody surface density and analyte antigen incubation time as dominant parameters influencing the antibody-antigen recognition events of a non-faradaic and diffusion-restricted electrochemical immunosensor. *Anal. Bioanal. Chem.* **2020**, *412*, 1709–1717.

https://doi.org/10.1021/acssensors.5c04140
ACS Sens. 2026, 11, 1655–1662